Remote Sensing of Environment 171 (2015) 105–117

Contents lists available at ScienceDirect

Remote Sensing of Environment

journal homepage: www.elsevier.com/locate/rse

Estimating the fraction of absorbed photosynthetically active radiation from the MODIS data based GLASS leaf area index product

Zhiqiang Xiao [a], Shunlin Liang [a,b], Rui Sun [a], Jindi Wang [a], Bo Jiang [a]

[a] State Key Laboratory of Remote Sensing Science, School of Geography, Beijing Normal University, Beijing 100875, China
[b] Department of Geographical Sciences, University of Maryland, College Park, MD 20742, USA

ARTICLE INFO

Article history:
Received 30 September 2014
Received in revised form 9 October 2015
Accepted 22 October 2015
Available online xxxx

Keywords:
GLASS products
FAPAR
LAI
Validation

ABSTRACT

The fraction of absorbed photosynthetically active radiation (FAPAR) is an essential biophysical variable and plays a critical role in the carbon cycle. Existing FAPAR products from satellite observations are spatially incomplete and temporally discontinuous, and also insufficiently accurate to meet the requirements of various applications. In this study, a new method is proposed to calculate high quality, accurate FAPAR from the Global LAnd Surface Satellite (GLASS) leaf area index (LAI) to ensure physical consistency between LAI and FAPAR retrievals. As a result, a global FAPAR product (denoted by GLASS) was generated from the GLASS LAI data from 2000. With no missing values, GLASS FAPAR product is spatially complete. Comparison of the GLASS FAPAR product with the MODerate Resolution Imaging Spectroradiometer (MODIS), Geoland2/BioPar version 1 (GEOV1), and the Sea-viewing Wide Field-of-view Sensor (SeaWiFS) FAPAR products indicates that these FAPAR products exhibit similar spatial distribution pattern. However, there were relatively large discrepancies between these FAPAR products in equatorial forest regions and around 50–60°N, where the SeaWiFS FAPAR values were lower than the other products and GLASS FAPAR product showed the largest values. Temporal consistency analysis indicates that GLASS FAPAR product has continuous trajectories, while MODIS FAPAR product shows more unstable profiles, especially during the growing season. Direct comparison with ground-based estimates demonstrated that GLASS FAPAR values were more accurate ($R^2 = 0.9292$ and RMSE $= 0.0716$) than GEOV1 ($R^2 = 0.8681$ and RMSE $= 0.1085$), MODIS ($R^2 = 0.8048$ and RMSE $= 0.1276$) and SeaWiFS FAPAR values ($R^2 = 0.7377$ and RMSE $= 0.1635$).

1. Introduction

The fraction of absorbed photosynthetically active radiation (FAPAR) is generally defined as the fraction of solar radiation absorbed by vegetation in the 400–700 nm spectral range (Gower, Kucharik, & Norman, 1999). FAPAR expresses the energy absorption capacity of vegetation, plays a critical role in the carbon cycle, and is an essential climate variable identified by the Global Climate Observing System (GCOS). Satellite observations provide the only feasible way to estimate FAPAR at regional and global scales.

Many algorithms have been developed to retrieve FAPAR from satellite remote sensing data (Knyazikhin, Martonchik, Myneni, Diner, & Running, 1998; Gobron, Aussedat, & Pinty, 2006; Gobron, Pinty, et al., 2006; Plummer, Arino, Simon, & Steffen, 2006; Baret et al., 2007), and multiple global FAPAR products have been generated from data acquired by the Medium Resolution Imaging Spectrometer (MERIS) (Gobron, Pinty, Verstraete, & Govaerts, 1999; Gobron et al., 2007), the Sea-viewing Wide Field-of-view Sensor (SeaWiFS) (Gobron et al., 2001), the MODerate Resolution Imaging Spectroradiometer (MODIS) (Knyazikhin et al., 1998; Gobron, Aussedat, et al., 2006) and SPOT/VEGETATION (Baret et al., 2007; 2013).

In general, two types of algorithms are employed, empirical and physical methods. Empirical methods are based on statistical relationships between FAPAR and vegetation indices to retrieve FAPAR from remote sensing data. They are calibrated for distinct vegetation types using field measurements and concurrently acquired satellite images (Riado, Conde, & Minguez, 1998). The limitation of relationship based approaches is that the resulting formulas are influenced by vegetation type and soil background. Physical methods, on the other hand, are based on the inversion of canopy radiative transfer models describing the transfer of solar radiation in vegetation canopies. Most currently available global FAPAR products are generated with physically based retrieval algorithms (Knyazikhin et al., 1998; Gobron, Pinty, et al., 2006; Plummer et al., 2006; Baret et al., 2007). To capitalize on existing FAPAR products, Baret et al. (2013) developed an algorithm to generate the Geoland2/BioPar version 1 (GEOV1) FAPAR product from SPOT/VEGETATION data using back-propagation neural networks.

Nevertheless, currently available empirical and physical methods generally use only single phase remote sensing data to retrieve FAPAR values. A consequence of using limited information during the inversion process is that the FAPAR products generated by these methods are spatially incomplete and temporally discontinuous, and also insufficiently

http://dx.doi.org/10.1016/j.rse.2015.10.016
0034-4257/

accurate to meet the requirements of various applications. Camacho, Cernicharo, Lacaze, Baret, and Weiss (2013) evaluated the performance of MODIS, Carbon cycle and Change in Land Observational Products from an Ensemble of Satellites (CYCLOPES), SeaWiFS and GEOV1 FAPAR products and showed that the GEOV1 and CYCLOPES FAPAR products presented the higher percentage of missing values in the equatorial region and at high latitudes in the northern hemisphere, whereas the MODIS main algorithm retrievals presented the largest fraction of missing values in the equatorial area with values higher than 60% during the January–March and October–December periods. An evaluation of the performances of Multiangle Imaging SpectroRadiometer (MISR), MODIS, SeaWiFS, MERIS, and GEOV1 FAPAR products at the global scale indicated that the uncertainties of current satellite FAPAR products are still unable to meet the threshold accuracy requirements stipulated by the Global Climate Observing System (GCOS) (±0.05) (Tao, Liang, & Wang, 2015). These FAPAR products were particularly inaccurate for some vegetation types (Serbin, Ahl, & Gower, 2013). The low accuracy and poor quality, in many cases, among existing FAPAR products require improvements or new products. Furthermore, currently available empirical and physical methods are generally parameter-specific algorithms to separately retrieve land surface parameters from various types of sensor data, which results in a lack of physical consistency between current land surface parameter products (Xiao, Liang, Wang, Xie, et al., 2015; Huemmrich, Privette, Mukelabai, Myneni, & Knyazikhin, 2005).

To improve the quality and accuracy of satellite products, a Global LAnd Surface Satellite (GLASS) system was developed to generate five products: leaf area index (LAI), shortwave broadband albedo, longwave broadband emissivity, downwelling shortwave radiation, and photosynthetically active radiation (PAR) (Liang, Zhang, et al., 2013; Liang, Zhao, et al., 2013). The GLASS LAI product was retrieved from time-series MODIS and Advanced Very High Resolution Radiometer (AVHRR) surface reflectance data using general regression neural networks (GRNNs) (Xiao et al., 2014). Unlike existing neural network methods that use remote sensing data acquired only at a specific time to retrieve LAI, the GRNNs were trained using fused time series LAI values from MODIS and CYCLOPES LAI products and reprocessed time series MODIS/AVHRR reflectance. The reprocessed MODIS/AVHRR reflectance values from an entire year were input to the GRNNs to estimate the one-year LAI profiles. The GLASS LAI product is one of the longest duration (1981–2013) LAI products in the world. Extensive validations for all biome types demonstrate that the GLASS LAI product provides temporally continuous LAI profiles with much improved quality and accuracy compared to the current MODIS and GEOV1 LAI products (Xiao, Liang, Wang, Xiang, et al., 2015). In this study, a new method is proposed to generate global FAPAR products from the GLASS LAI data derived from MODIS surface reflectance data to ensure physical consistency between LAI and FAPAR retrievals. The quality and accuracy of the retrieved FAPAR values were compared with existing global FAPAR products and directly validated against ground-based FAPAR estimates.

Section 2 describes the GLASS LAI product, existing global FAPAR products, and FAPAR ground measurements. Section 3 outlines the method employed to calculate FAPAR values from the GLASS LAI product. A comparison between the retrieved FAPAR values from the GLASS LAI product and existing global FAPAR products, and a direct validation of the retrieved FAPAR values against ground-based FAPAR estimates are presented in Section 4. Section 5 provides brief conclusions.

2. Data

2.1. Satellite data sets

The GLASS LAI product was used to derive FAPAR products, and existing global FAPAR products (MODIS, GEOV1, and SeaWiFS) were compared with the FAPAR products proposed in this study. The main characteristics of the GLASS LAI product and the MODIS, GEOV1 and SeaWiFS FAPAR products are described below.

2.1.1. GLASS LAI product

The GLASS LAI product was generated and released by the Center for Global Change Data Processing and Analysis of Beijing Normal University (WWW1). It is also available from the Global Land Cover Facility (WWW2). It has a temporal resolution of 8 days and spans 1981–2013. For the period 1981–1999, AVHRR reflectance data from NASA's Land Long-Term Data Record (LTDR) project (Pedelty et al., 2007) were used to generate the LAI product, which was provided in a geographic latitude/longitude projection at spatial resolution of 0.05° (~5 km at the Equator). For the period 2000–2013, the LAI product was derived from MODIS surface reflectance data and provided in a sinusoidal projection at spatial resolution of 1 km (Xiao, Liang, Wang, Xiang, et al., 2015).

2.1.2. Global FAPAR products

The MODIS FAPAR product has been available since 2000 and is provided in a sinusoidal projection at 1 km spatial resolution and 8 day time step (Myneni et al., 2002). The latest version (collection 5) was used in this study and was downloaded from WWW3. The retrieval algorithm includes a main algorithm and a backup algorithm. The main algorithm is based on lookup tables simulated from a three dimensional radiative transfer model. When the main algorithm fails, the backup algorithm is used to estimate FAPAR from biome specific relationships between FAPAR and normalized difference vegetation index (NDVI) (Knyazikhin et al., 1998). In collection 5, parameters of the main and backup algorithms are defined for eight main biome classes according to MODIS land cover, and a new stochastic radiative transfer model was employed to better represent canopy structure and the spatial heterogeneity intrinsic to woody biomes. Generally, FAPAR estimates using the backup algorithm are of lower quality, mainly because of residual clouds and poor atmospheric correction (Yang et al., 2006). The MODIS FAPAR product is defined as the instantaneous black sky FAPAR (i.e. under direct illumination) at the time of the Terra overpass (10:30 am).

The GEOV1 FAPAR product has been available since 1999 from WWW4. The product is provided in a Plate Carrée projection at 1/112° spatial resolution and a 10-day frequency. The GEOV1 FAPAR product was derived from SPOT/VEGETATION sensor data using back-propagation neural networks. The MODIS and CYCLOPES FAPAR products were fused and scaled to generate 'best estimates' of FAPAR, which were used to train the back-propagation neural networks with the SPOT/VEGETATION top-of-canopy nadir reflectance values over the BELMANIP (Benchmark Land Multisite Analysis and Intercomparison of Products) network of sites (Baret et al., 2013). The calibrated neural networks were used to generate the GEOV1 FAPAR product from SPOT/VEGETATION top-of-canopy nadir reflectance data. The GEOV1 FAPAR product corresponds to the instantaneous black sky FAPAR by green parts at 10:15 am local time.

The SeaWiFS FAPAR product for the period 1997–2006 from the SeaWiFS data was downloaded from WWW5. The product was remapped into a global sinusoidal projection at 2.17 km and generated on a daily, 10 day, and monthly basis. The FAPAR algorithm was based on the concept of an optimized vegetation index proposed by Gobron, Pinty, et al. (2006). The SeaWiFS FAPAR product corresponds to the instantaneous FAPAR under direct illumination by green parts at the time of satellite overpass (12:05 pm).

2.2. Field measurement data

27 high-resolution FAPAR maps over 22 sites from the Validation of Land European Remote sensing Instrument (VALERI) project (WWW6) were collected to validate the accuracy of the FAPAR products proposed in this study and the MODIS, GEOV1, and SeaWiFS FAPAR products.

FAPAR ground measurements at the VALERI sites were calculated from digital hemispherical photos. The FAPAR ground measurements correspond to the fraction of intercepted PAR (FIPAR). The high-resolution FAPAR maps were derived from the determination of the transfer function between the reflectance values of the high spatial resolution satellite imagery and the FAPAR ground measurements. The high-resolution FAPAR maps at all sites except for the FAPAR maps at the Fundulea site in 2003 and at the Gnangara site in 2004 have a spatial resolution of 20 m. The spatial resolution of the FAPAR map for the Fundulea site in 2003 is 10 m, while the spatial resolution of the FAPAR map for the Gnangara site in 2004 is 30 m. These high-resolution FAPAR maps were aggregated to medium resolution for comparison (Morisette et al., 2006). The characteristics of the validation sites and associated mean values of the high-resolution FAPAR maps over 3 km × 3 km regions centered on the location of the sites are shown in Table 1, and they were also reported in Camacho et al. (2013).

In addition, seven years of continuous ground measurements from the Bartlett experimental forest site (44.0646°N, 71.2881°W) of the AmeriFlux network were employed to validate these FAPAR products. Four components, incoming and outgoing solar flux, and flux from and to the ground, were measured at half hour intervals at this site. FAPAR ground measurements were calculated as the ratio of absorbed photosynthetically active radiation and incoming solar flux. To validate the FAPAR products, FAPAR values from these products should be compared with the ground measurements at the satellite observation times. Considering ground measurement errors, the average of the ground measurements within a 3 h window centered at 10:30 am for each day was calculated as the comparator for the FAPAR values from these products. Heterogeneity analysis using Landsat images demonstrated that the area around the Bartlett site was, in general, homogeneous with respect to vegetation intensity (Tao et al., 2015).

In fact, there are two types of ground-based FAPAR measurements. Huemmrich et al. (2005) have demonstrated that there was very little difference in values between FIPAR and FAPAR. The largest difference was around 4% FAPAR. The small difference between intercepted and absorbed PAR was because an increase in PAR coming into the canopy through reflectance from the ground was just about offset by the above canopy reflected PAR (Huemmrich et al., 2005).

3. Methodology

Solar radiation provides the energy for photosynthetic activity required for vegetation growth. The photosynthetically active radiation (PAR, 400–700 nm) incident on a vegetation canopy enters the canopy from both above and below the canopy, leaves the canopy into the upward and downward hemispheres, enters or exits the vegetation canopy laterally, and is absorbed by the canopy.

In terms of the energy balance of a vegetation canopy, FAPAR is the difference of the total (direct and diffuse) PAR into and out of the vegetation canopy divided by incoming PAR,

$$FAPAR = \frac{PAR_{ci} - PAR_{cr} + PAR_{sr} - PAR_{si} + \Delta PAR_H}{PAR_{ci}}, \quad (1)$$

where PAR_{ci} is the incoming PAR above the canopy, PAR_{cr} is the PAR reflected from the canopy, PAR_{si} is the incident below-canopy PAR after being intercepted by leaves, PAR_{sr} is the PAR reflected from the soil under the canopy, and ΔPAR_H is the net PAR entering and exiting the canopy laterally. Eq. (1) can be expressed as

$$FAPAR = 1 - \alpha - \tau_{PAR} + \tau_{PAR}\alpha_s + f^H_{netPAR}, \quad (2)$$

where α is the albedo of the visible band at the top of the vegetation canopy, α_s is the soil albedo, $\tau_{PAR} = \frac{PAR_{si}}{PAR_{ci}}$ is the transmittance of the PAR down to the soil, and $f^H_{netPAR} = \frac{\Delta PAR_H}{PAR_{ci}}$ is the normalized contribution of net PAR entering and exiting the canopy laterally.

The FAPAR values can be calculated using Eq. (2) if α, α_s, τ_{PAR} and f^H_{netPAR} are known. Widlowski, Lavergne, Pinty, and Gobron (2008) showed that the contribution of f^H_{netPAR} in Eq. (2) decreases with the spatial extent of the canopy. Therefore, this effect is small and was ignored when calculating FAPAR values for the medium resolution pixels in our study. Nevertheless, it is also difficult to obtain high quality data sets for the other parameters, especially for α_s at a regional or global scale,

Table 1
Characteristics of the 22 validation sites.

Site name	Country	Latitude (°)	Longitude (°)	Biome type	DOY	Year	Mean FAPAR[a]	Uncertainties of FAPAR
Alpilles2	France	43.810	4.715	Broadleaf crops	204	2002	0.399	0.292
Barrax	Spain	39.057	−2.104	Broadleaf crops	194	2003	0.256	0.333
Cameron	Australia	−32.598	116.254	Broadleaf forest	63	2004	0.479	0.109
Concepcion	Chile	−37.467	−73.470	Broadleaf forest	9	2003	0.771	0.197
Counami	French Guyana	5.347	−53.238	Broadleaf forests	269	2001	0.95	0.006
					286	2002	0.887	0.005
Demmin	Germany	53.892	13.207	Broadleaf crops	164	2004	0.741	0.207
Donga	Benin	9.770	1.778	Shrubs	172	2005	0.472	0.159
Fundulea	Romania	44.406	26.583	Grasses and cereal crops	128	2001	0.519	0.370
					160	2002	0.464	0.269
					151	2003	0.374	0.221
Gilching	Germany	48.082	11.320	Grasses and cereal crops	199	2002	0.786	0.201
Gnangara	Australia	−31.534	115.882	Broadleaf forest	61	2004	0.263	0.058
Haouz	Morocco	31.659	−7.600	Shrubs	71	2003	0.489	0.252
Laprida	Argentina	−36.990	−60.553	Savannahs	311	2001	0.837	0.102
					292	2002	0.62	0.040
Larose	Canada	45.380	−75.217	Needleleaf forests	219	2003	0.906	0.080
Larzac	France	43.938	3.123	Savannahs	183	2002	0.349	0.059
Nezer	France	44.568	−1.038	Needleleaf forests	107	2002	0.494	0.269
Plan-de-Dieu	France	44.199	4.948	Broadleaf crops	189	2004	0.223	0.120
Puechabon	France	43.725	3.652	Broadleaf forests	164	2001	0.601	0.157
Sonian	Belgium	50.768	4.411	Needleleaf forests	174	2004	0.916	0.036
Sud-Ouest	France	43.506	1.238	Grasses and cereal crops	189	2002	0.404	0.258
Turco	Bolivia	−18.239	−68.193	Shrubs	240	2002	0.025	0.013
					105	2003	0.046	0.016
Wankama	Niger	13.645	2.635	Grasses and cereal crops	174	2005	0.073	0.057
Zhangbei	China	41.279	114.688	Grasses and cereal crops	221	2002	0.422	0.143

[a] The FAPAR ground measurements correspond to the fraction of intercepted PAR.

although various methods have been developed to estimate them from remote sensing data (Rechid, Raddatz, & Jacob, 2009; Carrer et al., 2014; Pinty et al., 2011).

In this study, a simple scheme is proposed to calculate FAPAR values from the GLASS LAI product to ensure physical consistency between LAI and FAPAR retrievals.

$$FAPAR = 1 - \tau_{PAR}. \quad (3)$$

The scheme ignores $\tau_{PAR}\alpha_s - \alpha$ in Eq. (2), and uses only the transmittance of PAR down to the soil to calculate the approximate FAPAR. The radiation into the vegetation canopy includes direct and diffuse PAR. Therefore, the transmittance of the PAR down to the soil is further expressed as

$$\tau_{PAR} = \tau_{PAR}^{dir} - \left(\tau_{PAR}^{dir} - \tau_{PAR}^{dif}\right) \times f_{skyl}, \quad (4)$$

where τ_{PAR}^{dir} and τ_{PAR}^{dif} are the fraction of the radiative flux originating from the direct illumination source and the transmitted fraction of the incident diffuse illumination source, respectively; f_{skyl} is the fraction of diffuse sky light, and varies with aerosol optical depth, solar zenith angle, band wavelength, and aerosol model type. In our study, f_{skyl} was calculated using a look-up table established from the Second Simulation of the Satellite Signal in the Solar Spectrum (6S) code (WWW7).

The canopy transmittance is closely related to sun zenith angle, the amount of diffuse radiation, and canopy clumping. If the leaf area index of a canopy is *lai* and the absorptivity of leaves for radiation is *a*, Campbell and Norman (1998) showed that the fraction of the total beam radiation (direct and down scattered) transmitted through the canopy can be approximated using an exponential model,

$$\tau_{PAR}^{dir} = e^{-\sqrt{a}\times k_c(\varphi)\times\Omega\times lai}, \quad (5)$$

where Ω is the clumping index, φ is the solar zenith angle, and $k_c(\varphi)$ is the canopy extinction coefficient for PAR. For an ellipsoidal leaf angle distribution, $k_c(\varphi)$ is calculated as follows.

$$k_c(\varphi) = \frac{\sqrt{x^2 + \tan^2(\varphi)}}{x + 1.774 \times (x + 1.182)^{-0.733}}, \quad (6)$$

where *x* is the ratio of average projected areas of canopy elements on horizontal and vertical surfaces. Different values are assigned to *x* for different vegetation types. Diffuse radiation comes from all directions. Therefore, the diffuse transmission coefficient, τ_{PAR}^{dif}, can be calculated by integrating the direct transmission coefficient over all illumination directions,

$$\tau_{PAR}^{dif} = 2\int_0^{\frac{\pi}{2}} \tau_{PAR}^{dir} \sin\varphi\cos\varphi d\varphi. \quad (7)$$

To quantify the importance of the input parameters for Eq. (3) on FAPAR and characterize their effects, a sensitivity analysis of FAPAR to target composition and architecture was performed using the extended Fourier amplitude sensitivity test (EFAST) originally developed by Cukier, Fortuin, Schuler, Petschek, and Schaibly (1973); Cukier, Levine, and Schuler (1978) and extended by Saltelli, Tarantola, and Chan (1999). EFAST is a variance based method and has proven one of the most reliable methods among these techniques (Saltelli, 2004), although computationally expensive (Ratto, Pagano, & Young, 2007). It provides a first order and a total order sensitivity index for each input parameter. The first order sensitivity index expresses the additive effect of the corresponding input parameter, whereas the total order sensitivity index is the overall measure of importance and incorporates the interactions of the input parameters.

Table 2
Range of input parameters for formula (3).

Factors	Unit	Range of variation	Distribution
Leaf area index	m^2/m^2	[0, 8]	Uniform
Clumping index	–	[0.5, 1.0]	Uniform
Solar zenith angle	Degrees	[0, 90]	Uniform
Absorptivity of leaves	–	[0.5, 1.0]	Uniform
Ratio of average projected areas of canopy elements on horizontal and vertical surfaces	–	[0.5, 2.0]	Uniform

Various ranges of input parameters used to calculate FAPAR are shown in Table 2. An input sample of 29,967 combinations of input parameters was provided by EFAST and used to calculate 29,967 FAPAR values using (3). Sensitivity analysis was performed on this set of FAPAR values (see Fig. 1). The first order and total order indices of sensitivity analysis demonstrate that LAI is the only sensitive parameter. Therefore, FAPAR values calculated from Eq. (3) are primarily influenced by LAI of the vegetation canopy.

For the above scheme, LAI is an important input parameter to estimate FAPAR values. The GLASS LAI product was used to calculate the FAPAR values in this study. The clumping index is another input parameter. Based on the linear relationship between the clumping index and the normalized difference between hot-spot and dark-spot indexes, Chen, Menges, and Leblanc (2005) derived a global clumping index map using Polarization and Directionality of the Earth's Reflectances (POLDER) data at ~6 km resolution. Later, He, Chen, Pisek, Schaaf, and Strahler (2012) employed the MODIS bidirectional reflectance distribution function (BRDF) parameter to derive a global clumping index map at 500 m resolution. In the present study, the MODIS derived clumping index map was used to calculate canopy transmittance.

The scheme detailed above were used to calculate FAPAR at 10:30 a.m. local time, which are close approximations of daily average FAPAR (Fensholt, Sandholt, & Rasmussen, 2004). For clarification, FAPAR values derived from Eq. (3) are denoted by GLASS FAPAR.

4. Results analysis

The spatial and temporal consistencies of the GLASS FAPAR values derived from the GLASS LAI product are assessed by comparison with MODIS, GEOV1, and SeaWiFS FAPAR products, and the accuracy of the GLASS FAPAR values was evaluated against ground-based FAPAR estimates. Only valid FAPAR values of the various products were used for comparison and validation. For the GLASS, GEOV1, and SeaWiFS FAPAR products, all FAPAR values were considered to be valid. For the

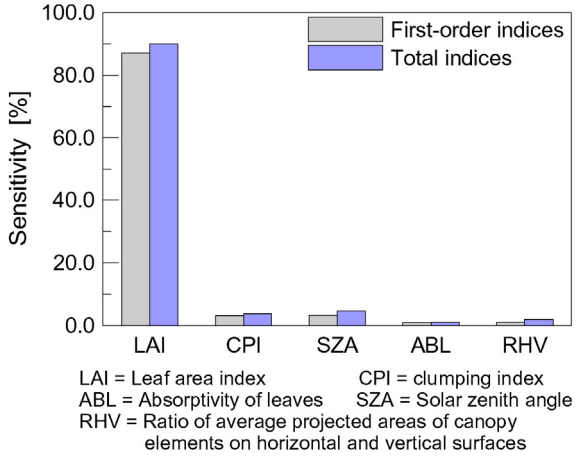

Fig. 1. First order and total order indices of sensitivity analysis for Eq. (3).

MODIS FAPAR product, only those values retrieved from the main algorithm were considered to be valid because of the overall lower quality for the FAPAR values produced by the backup algorithm (Yang et al., 2006).

4.1. Comparison with existing FAPAR products

4.1.1. Spatial consistency

For comparisons of spatial consistency, all the FAPAR products were re-projected onto the geographic latitude/longitude projection using

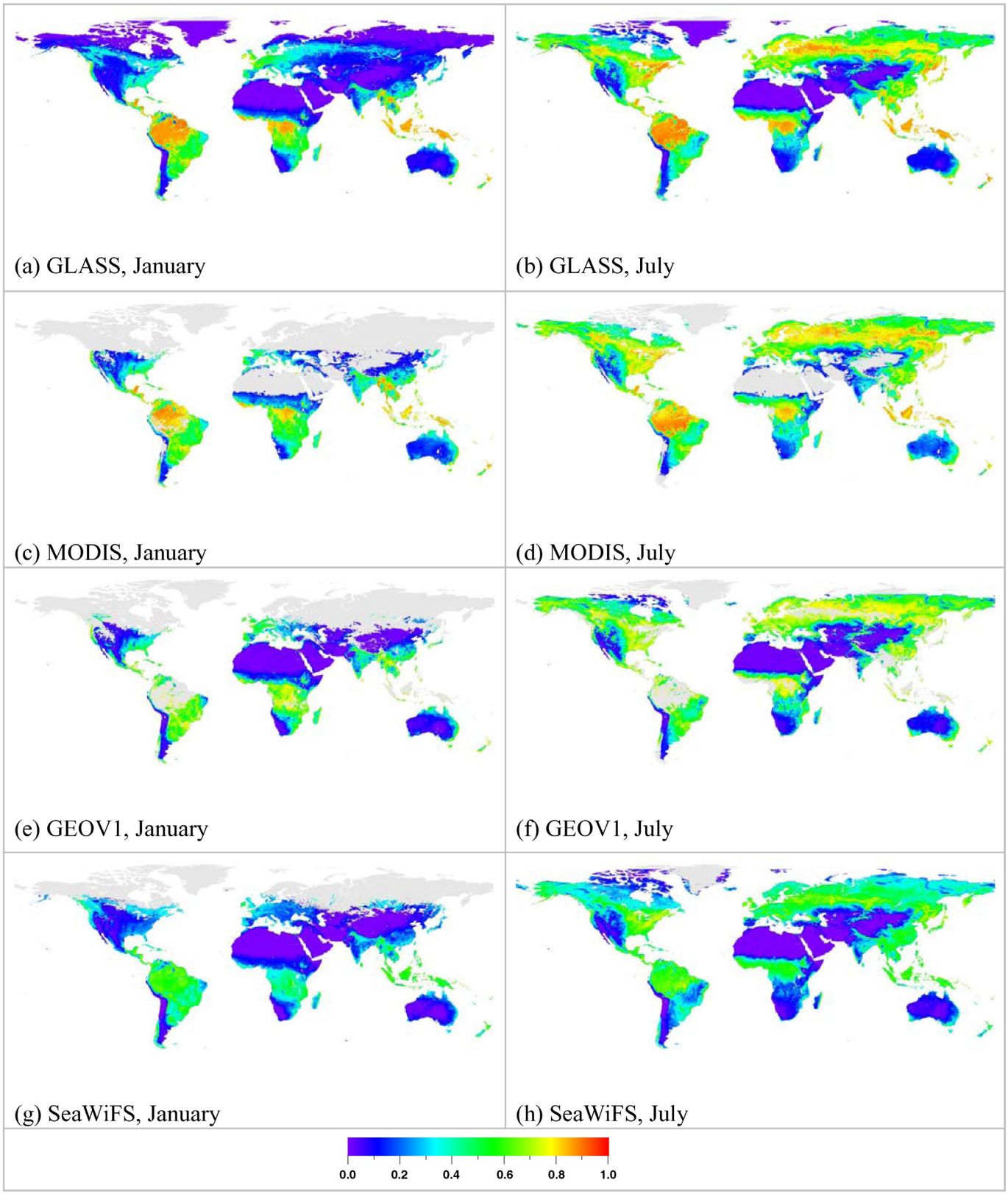

Fig. 2. Global mean FAPAR for GLASS, MODIS, GEOV1, and SeaWiFS products from 2001 to 2005. Left panels: January. Right panels: July.

nearest-neighbor resampling and were aggregated to 0.25° resolution using spatial averaging. The average value over a 0.25° pixel was computed if more than 70% of the pixels projected into the 0.25° pixel had valid FAPAR values. The FAPAR products were then aggregated into a monthly time step by computing the monthly average from the valid FAPAR values.

To investigate spatial patterns specific to a given product as well to check the distribution in space of missing data, global maps of the mean values for the GLASS, MODIS, GEOV1 and SeaWiFS FAPAR products were calculated for January and July 2001–2005, as shown in Fig. 2. Areas masked in gray correspond to pixels where the FAPAR product did not provide valid values. MODIS, GEOV1, and SeaWiFS FAPAR products have missing pixels in rainforest regions and in mid and high latitude zones of the northern hemisphere, especially in January. However, there are no missing data for the GLASS FAPAR product, because the retrieval algorithm uses the spatially and temporally complete GLASS LAI product.

The various FAPAR products are generally consistent in their spatial patterns. Higher FAPAR values are produced over equatorial forest regions and around 50–60°N, whereas they are intermediate at mid and high latitude zones, and very low over sparsely vegetated areas. However, discrepancies are evident in the relative magnitude of the FAPAR products. There is a relatively large discrepancy in equatorial forest regions and around 50–60°N, where SeaWiFS FAPAR values are lower than the values from other products and GLASS product has the largest FAPAR values. The discrepancies among these products are partly explained by the definition of FAPAR used in each dataset. It is normal that the total FAPAR is higher than direct one. The algorithm assumption is another factor that can lead to these differences in these FAPAR products (D'Odorico et al., 2014).

Density scatterplots between the GLASS, MODIS, GEOV1, and SeaWiFS FAPAR values around the globe during 2001–2005 are shown in Fig. 3. The regression in Fig. 3a has a slope less than one (0.9151) and a positive intercept (0.0764), which demonstrates that the MODIS FAPAR values are slightly larger than those of GLASS for low FAPAR values. Fig. 3b and d show that the GEOV1 FAPAR values are lower than those of GLASS, and MODIS for low FAPAR values. The majority of points in Fig. 3c, e and f are below the 1:1 line, which indicates that SeaWiFS FAPAR values are systematically lower than those of GLASS, MODIS, and GEOV1, a result which is in agreement with the findings of McCallum et al. (2010) and Camacho et al. (2013). These discrepancies should be partly explained by the later overpass time of SeaWIFS corresponding to lower solar zenith angles, but probably also by a lack of representativeness of the training data base used to calibrate the algorithm (Camacho et al., 2013).

Statistical distributions of the FAPAR values for 2001–2005, as shown in Fig. 4, were generated for each biome type according to the MODIS land cover type to illustrate the similarities and differences between these FAPAR products. The SeaWiFS product has significantly different distributions of FAPAR values from the other products as observed previously. The SeaWiFS FAPAR values are systematically lower, especially for savannah and the four forest biome types. For the evergreen broadleaf forest biome type, GLASS, MODIS, and GEOV1 FAPAR products all have distributions with a narrow peak, but the GLASS and MODIS frequency distribution peaks (approximately 0.8) are larger than those of GEOV1, and SeaWiFS.

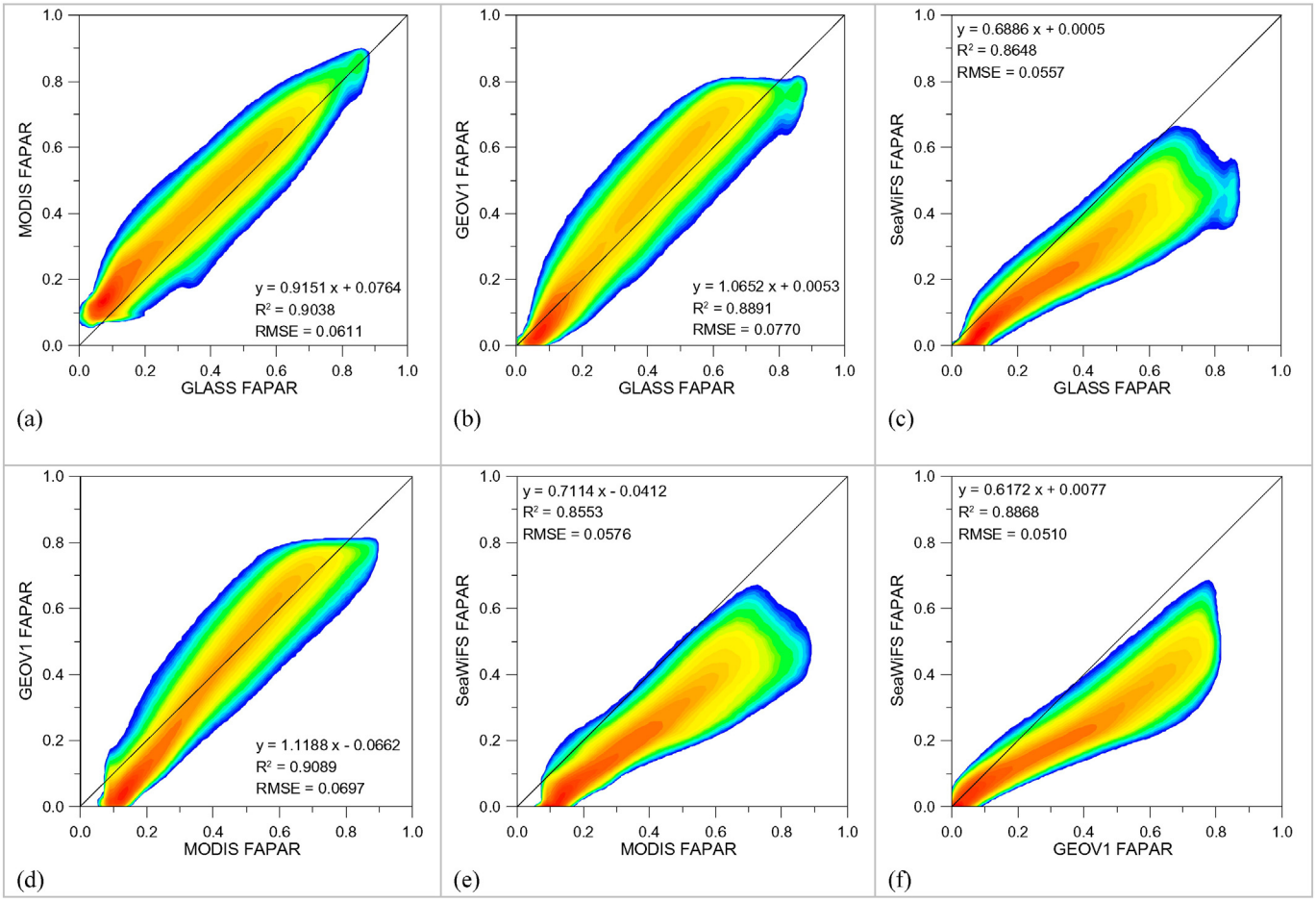

Fig. 3. Density scatterplots between the GLASS, MODIS, GEOV1, and SeaWiFS FAPAR values around the globe during 2001–2005. The GLASS FAPAR values correspond to total FAPAR, while the MODIS, GEOV1 and SeaWiFS FAPAR values correspond to direct FAPAR.

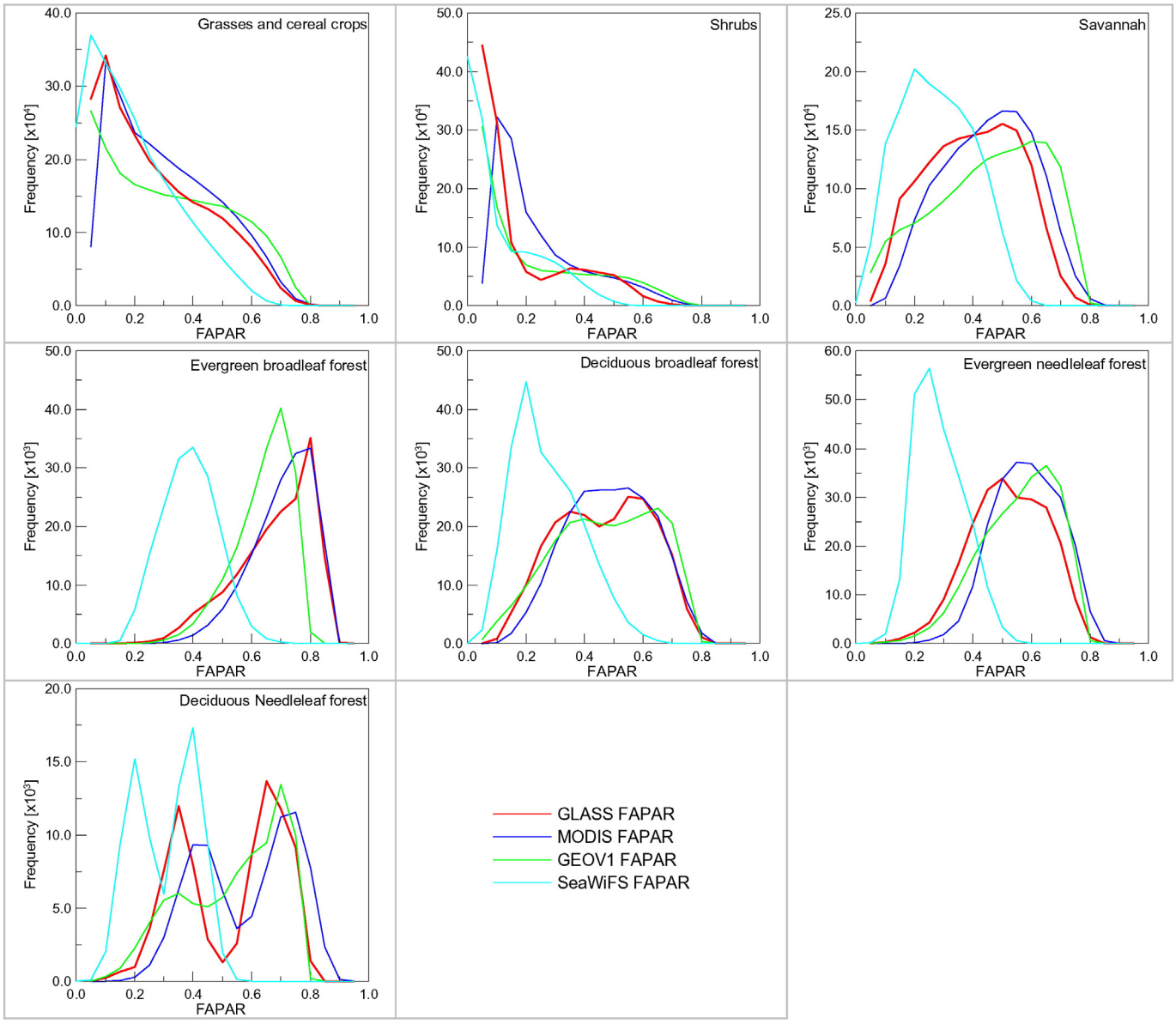

Fig. 4. Histograms of the GLASS, MODIS, GEOV1, and SeaWiFS FAPAR products for 2001–2005 for different biome types.

To quantitatively assess the main discrepancies between these FAPAR products, the differences among these FAPAR products were computed as a function of latitude and biome type. Fig. 5 shows mean values of the FAPAR differences for different 10°-latitude bands in each month for 2001–2005. In most latitude bands for each month, the mean FAPAR differences between GLASS and MODIS, GEOV1 FAPAR products are negative (Fig. 5a and b), indicating that the GLASS FAPAR values for these regions are slightly smaller than the corresponding MODIS and GEOV1 FAPAR values. However, the GLASS FAPAR values were larger than those of MODIS and GEOV1 in rainforest regions along the Equator. The SeaWiFS FAPAR values were smaller than those of all other products for each month, especially in the equatorial forest regions and around 55–65°N latitude (Fig. 5c, e and f).

Fig. 6 shows mean values of the FAPAR differences for different biome types in each month for 2001–2005. GLASS FAPAR values are smaller than those of MODIS for all biome types except shrubs, evergreen and deciduous broadleaf forests in all months. For the deciduous broadleaf forest, mean values of the FAPAR differences between GLASS and MODIS FAPAR products are positive only in June and September. GLASS FAPAR values are larger than those of MODIS in May–August for evergreen broadleaf forest, where GLASS and MODIS FAPAR products also show the best consistency, with maximum mean FAPAR difference of only 0.019 in February. The largest difference between GLASS and MODIS FAPAR products is for deciduous needleleaf forests in February, where the GLASS FAPAR value is 0.193 less than those of MODIS.

Mean values of the FAPAR differences between GLASS and GEOV1 FAPAR products are negative for grasses and cereal crops, and savannah in all months; whereas GLASS FAPAR values are almost 0.07 larger than those of GEOV1 for evergreen broadleaf forest in all months. GLASS and GEOV1 FAPAR products show good consistency for grasses and cereal crops, shrubs, and deciduous broadleaf forest especially in January, February, and March.

The mean FAPAR differences between GLASS and SeaWiFS FAPAR product are significantly larger than those between GLASS and other FAPAR products for all vegetation classes, confirming the previous observations. GLASS FAPAR values are higher than those of SeaWiFS for all biome types in all months. The mean FAPAR differences for the forest biomes were generally larger than those for other biome types. The largest difference between GLASS and SeaWiFS FAPAR products is for

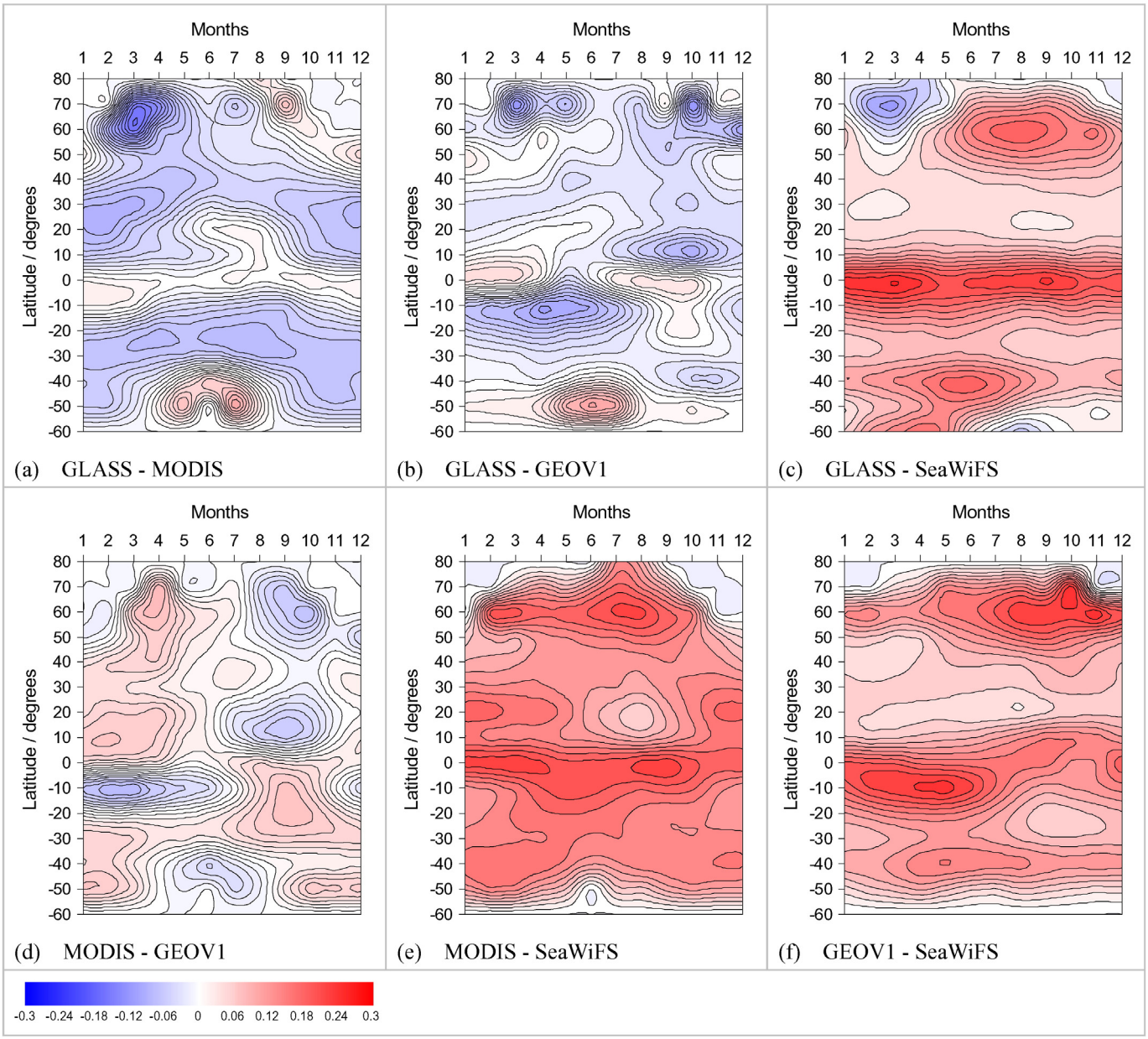

Fig. 5. Hovmoller diagrams of mean values of the FAPAR differences among GLASS, MODIS, GEOV1 and SeaWiFS FAPAR products for different 10°-latitude bands in each month for 2001–2005. The GLASS FAPAR values correspond to total FAPAR, while the MODIS, GEOV1 and SeaWiFS FAPAR values correspond to direct FAPAR.

evergreen broadleaf forests where GLASS FAPAR values are almost 0.323 larger than those of SeaWiFS.

4.1.2. Temporal consistency

Temporal consistency was evaluated between GLASS, MODIS, GEOV1, and SeaWiFS FAPAR products over a sample of VALERI sites with different biome classes. Detailed information about the sites and mean values of the high resolution FAPAR maps over the 3 km × 3 km regions centered on the location of the sites are given in Table 1.

For comparison of temporal consistency, the original product temporal resolution (8 day for MODIS and GLASS and 10 day for GEOV1 and SeaWiFS) was considered for each FAPAR product. Average FAPAR profiles for the GLASS, MODIS, and GEOV1 FAPAR products over 3 × 3 pixels centered on the selected sites were calculated to reduce effects from co-registration errors between them. The average FAPAR value over the 3 × 3 pixels was computed if there were more than five valid values among the nine pixels (Camacho et al., 2013). The average FAPAR profiles over one year were compared for each site to provide a qualitative assessment of seasonal variations between the products. The specific years used for comparison were not the same for all sites, but varied according to the availability of the high resolution FAPAR maps derived from ground measurements. These FAPAR profiles were also compared with the mean values of the high resolution FAPAR maps to analyze the precision of each product in the time series.

Temporal profiles of the FAPAR products for the selected sites are shown in Fig. 7. GLASS FAPAR profiles show the best temporal continuity, followed by GEOV1 profiles, whereas MODIS and SeaWiFS profiles show many fluctuations, especially during the growing season. SeaWiFS FAPAR values are systematically lower than those of the other products for most sites.

The temporal FAPAR trajectories for the Gilching and Zhangbei sites with grass and cereal crop biome types are shown in Fig. 7a. For the Gilching site, there is good agreement among the GLASS, GEOV1 and MODIS FAPAR values for 2002, whereas the SeaWiFS FAPAR values are significantly lower throughout the year and underestimate the mean value of the high resolution FAPAR map. For the Zhangbei site, the

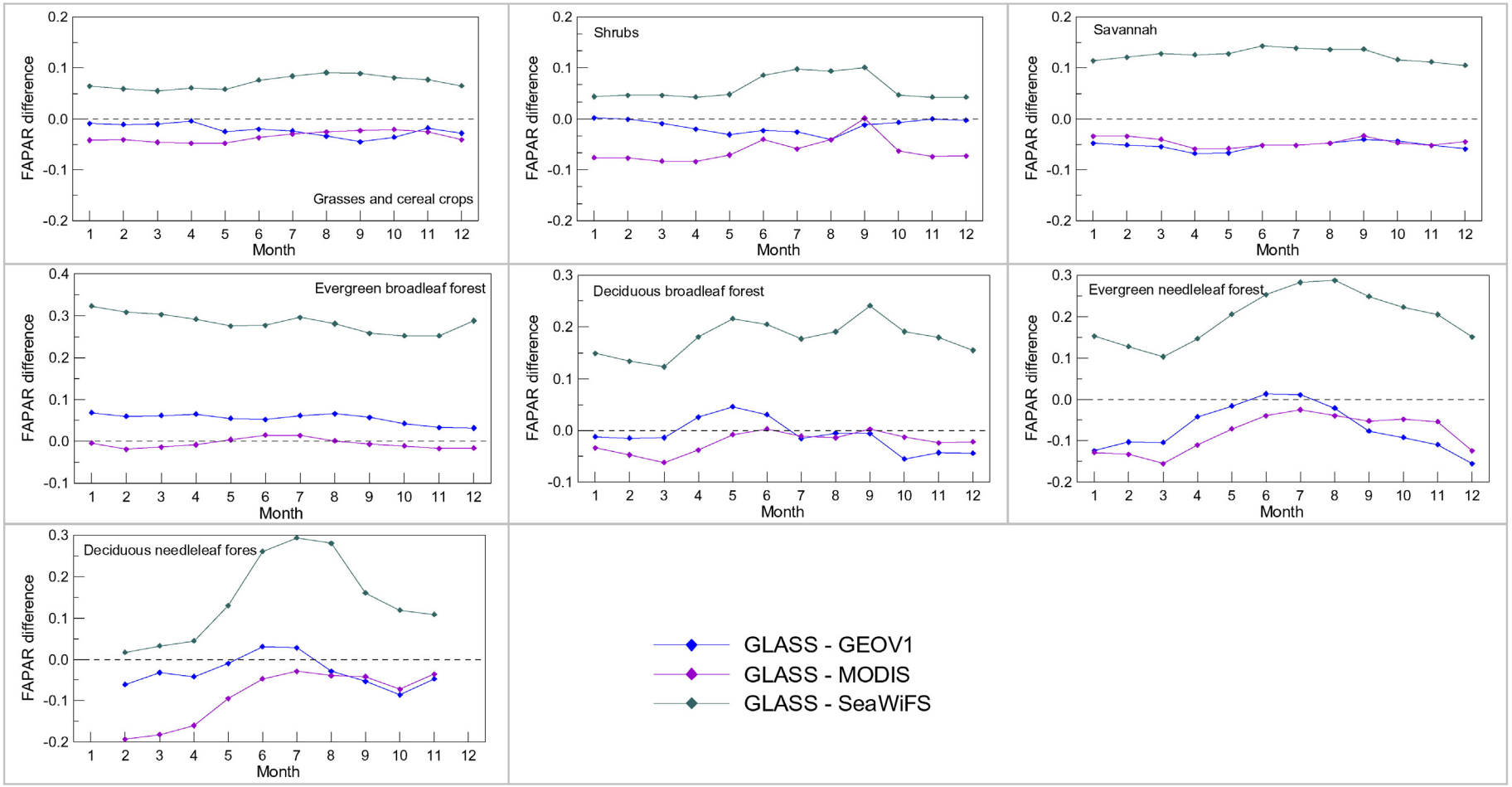

Fig. 6. Mean values of the FAPAR differences among GLASS, MODIS, GEOV1 and SeaWiFS FAPAR products for different biome types in each month for 2001–2005.

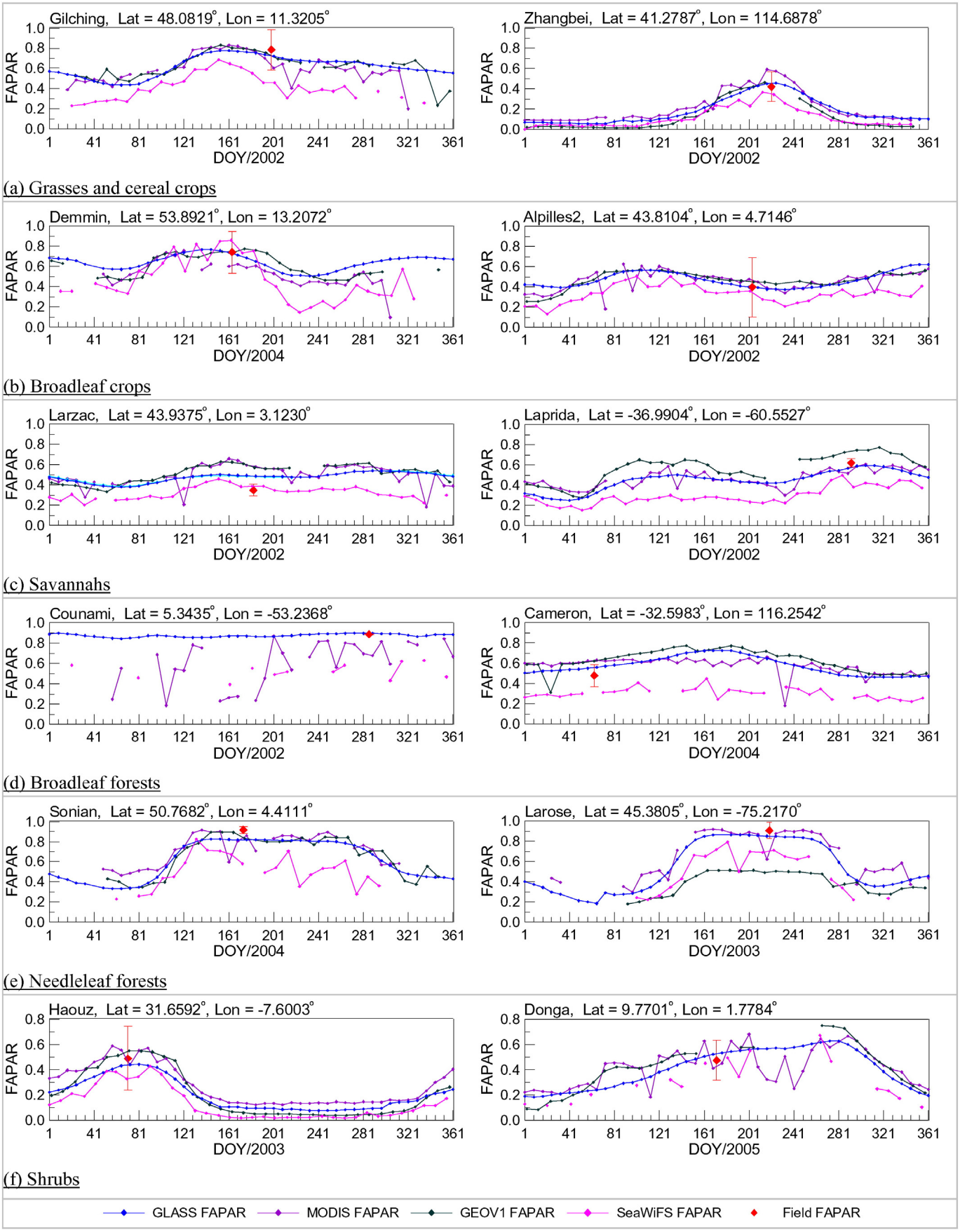

Fig. 7. Temporal profiles of the GLASS, MODIS, GEOV1 and SeaWiFS FAPAR values for several sites with different vegetation types.

GLASS FAPAR profile is in good agreement with that of MODIS during the whole year, whereas the GEOV1 and SeaWiFS FAPAR values are slightly smaller than those of GLASS through the non-growing season.

The temporal FAPAR profiles for the Demmin and Apilles2 sites (broadleaf crop biome) are shown in Fig. 7b. For the Demmin site, GLASS FAPAR values agree with those of GEOV1, MODIS, and SeaWiFS during the growing season, but are slightly larger than the GEOV1 and MODIS FAPAR values during the non-growing season. For the Apilles2 site, the GLASS FAPAR profile agrees with those of GEOV1 and MODIS. However, GLASS FAPAR values are more accurate than those of MODIS and GEOV1 compared to the mean value of the high resolution FAPAR map at this site.

The temporal FAPAR profiles for the Larzac and Laprida sites (savannah biome) are shown in Fig. 7c. For the Larzac site, the MODIS FAPAR profile agrees well with that of GEOV1 during the whole year. SeaWiFS FAPAR values are significantly lower than GLASS, GEOV1, and MODIS FAPAR values, but closer to the mean value of the high resolution FAPAR map. For the Laprida site, the GLASS FAPAR profile agrees well with MODIS FAPAR profile. During the growing season, GEOV1 FAPAR values are larger than those of GLASS, MODIS, and SeaWiFS at this site.

The temporal LAI trajectories for broadleaf forest sites are shown in Fig. 7d. There are large discrepancies for the Counami site. The GEOV1 FAPAR values during the whole year are missing and most SeaWiFS FAPAR values are also missing. The MODIS FAPAR profile shows dramatic fluctuations, whereas GLASS FAPAR values have continuous trajectories. The GLASS FAPAR values are approximately constant for the entire year and are higher than those of MODIS, GEOV1 and SeaWiFS. For the Cameron site, the GLASS FAPAR profile is in good seasonality agreement with those of GEOV1, MODIS, and SeaWiFS. During the whole year, the GEOV1 FAPAR values are higher than those of GLASS and MODIS, whereas the SeaWiFS values are significantly lower than those of GLASS and MODIS. In contrast, the GLASS FAPAR values are closer to the mean value of the high resolution FAPAR map for the Counami and Cameron sites.

The temporal FAPAR trajectories for needleleaf forest biome sites are shown in Fig. 7e. For the Sonian site, the temporal FAPAR trajectories of GLASS, MODIS, and GEOV1 show good agreement during the 2004 growing season and are close to the mean value of the high resolution FAPAR map. Aside from fluctuations, SeaWiFS FAPAR values are significantly smaller than those of the other FAPAR products at this site. For the Larose site, GLASS, and MODIS FAPAR values have almost the same magnitude, while GEOV1 FAPAR values are systematically lower during the growing seasons.

The temporal FAPAR trajectories for the shrub biome sites (Fig. 7f) show similar seasonal variations. For the Haouz site, MODIS and GEOV1 FAPAR values are slightly higher than those of GLASS, and SeaWiFS during the growing season. For the Donga site, the MODIS FAPAR profile shows significant fluctuations and most SeaWiFS FAPAR values are missing during the growing season. The GLASS FAPAR profile achieves good agreement with the envelope of the time series MODIS FAPAR values and are closer to the mean value of the high resolution FAPAR map in 2005.

Fig. 8 shows the temporal profiles of the FAPAR ground measurements and GLASS, MODIS, GEOV1, and SeaWiFS FAPAR values at the Bartlett experimental forest site from 2004 to 2010. The satellite derived FAPAR products at 1 km resolution are compared with the ground measurement time series. The seasonality exhibited by ground measurements and satellite FAPAR products show excellent agreement for these years although the FAPAR ground measurements have a lot of noise. The MODIS FAPAR profile has some fluctuations. During the vegetation growing season, the GEOV1 FAPAR values are slightly higher than GLASS and MODIS FAPAR values. GLASS, GEOV1 and MODIS FAPAR values agree better with ground measurements in magnitudes than SeaWiFS FAPAR values although the FAPAR values of these products all underestimate FAPAR ground measurements during the growing season at this site.

4.2. Direct validation

The GLASS, MODIS, GEOV1, and SeaWiFS FAPAR products were compared with high-resolution FAPAR maps to evaluate differences in FAPAR magnitude between the products. The high-resolution FAPAR maps and the GLASS, MODIS, and GEOV1 FAPAR products were aggregated over 3 km × 3 km regions centered on the location of the validation sites using spatial averaging. GLASS, MODIS, GEOV1, and SeaWiFS FAPAR values were linearly interpolated to the acquisition date of FAPAR ground measurements if the two closest FAPAR values were within ±10 days from that date. A total of 22 sites, providing 27 high resolution FAPAR maps were retained for which GLASS, GEOV1, MODIS, or SeaWiFS FAPAR products provided valid data.

Scatterplots of the FAPAR products versus the mean values of the high-resolution FAPAR maps are shown in Fig. 9. All the FAPAR products underestimate high FAPAR values and overestimate low FAPAR values compared to the mean values of the high-resolution FAPAR maps. GLASS FAPAR product provide the greatest accuracy ($R^2 = 0.9292$ and RMSE $= 0.0716$) against the mean values of the high-resolution FAPAR maps compared to GEOV1 ($R^2 = 0.8681$ and RMSE $= 0.1085$), MODIS ($R^2 = 0.8048$ and RMSE $= 0.1276$), and SeaWiFS FAPAR products ($R^2 = 0.7377$ and RMSE $= 0.1635$).

Compared with MODIS, GEOV1, and SeaWiFS FAPAR values, those of GLASS are distributed more closely around the 1:1 line against the mean values of the high-resolution FAPAR maps, showing that GLASS FAPAR

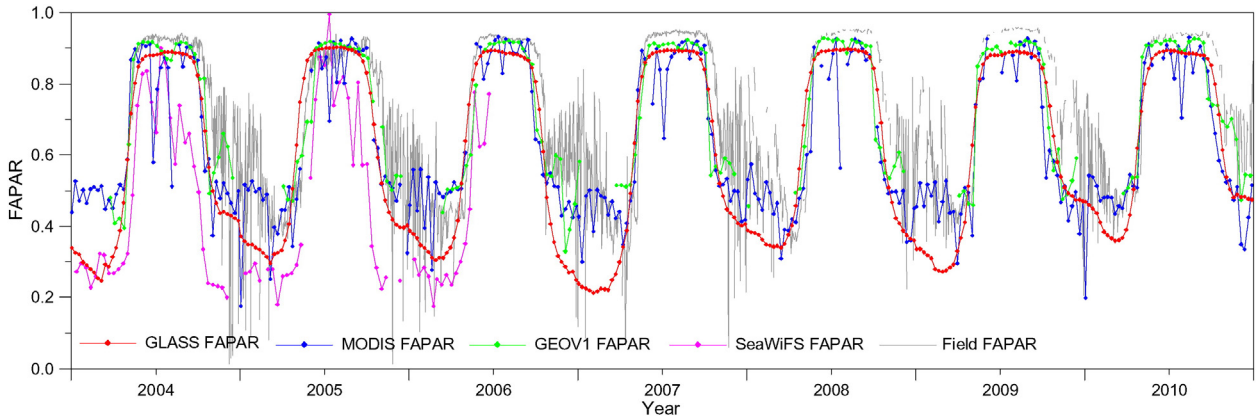

Fig. 8. Time series of FAPAR ground measurements and satellite FAPAR products at the Bartlett experimental forest site 2004–2010. The GLASS FAPAR values correspond to total FAPAR, while the MODIS, GEOV1 and SeaWiFS FAPAR values correspond to direct FAPAR.

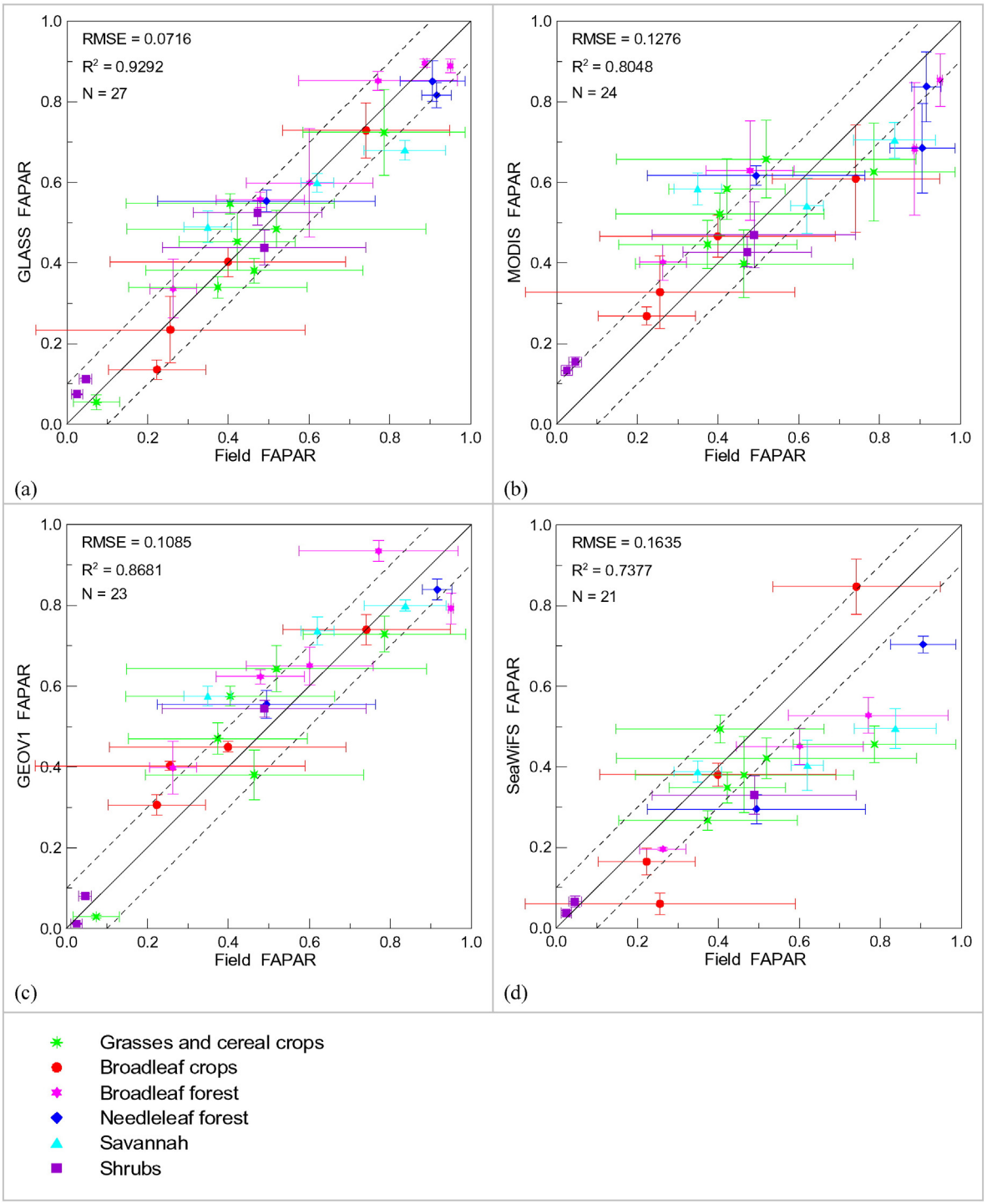

Fig. 9. Scatterplots of (a) GLASS, (b) MODIS (c) GEOV1and (d) SeaWiFS FAPAR products versus mean values of the high resolution FAPAR maps. The R-squared and RMSE values are also shown. N is the number of matched data pairs for each case.

product achieves better agreement with the mean values of the high-resolution FAPAR maps across the FAPAR range than the other products.

5. Conclusions

A new method is proposed to generate physically consistent FAPAR values from GLASS LAI. The quality and accuracy of the generated FAPAR product (GLASS) were evaluated by comparison with MODIS, GEOV1, and SeaWiFS FAPAR products and directly validated against ground-based FAPAR estimates.

Comparison with MODIS, GEOV1, and SeaWiFS FAPAR products showed that all the FAPAR products were generally consistent in their spatial patterns. However, there were relatively large discrepancies between the various FAPAR products in equatorial forest regions and around 50–60°N, where the SeaWiFS FAPAR values were significantly lower than those of the other products, and GLASS FAPAR product had the largest values.

The temporal profiles of the FAPAR products showed consistent seasonal variations. GLASS FAPAR product had continuous trajectories, while MODIS FAPAR product had less stable profiles, especially during

growing seasons. Direct comparison with ground-based estimates showed that GLASS FAPAR product provided the greatest accuracy against the mean values of high resolution FAPAR maps.

The proposed methods were used to calculate FAPAR values based on GLASS LAI derived from MODIS reflectance data. In the near future, the authors will extend this to calculate FAPAR values based on GLASS LAI derived from AVHRR reflectance data and perform more extensive validation and analysis of GLASS FAPAR values.

Acknowledgments

The GLASS LAI product is generated and released by the Center for Global Change Data Processing and Analysis of Beijing Normal University (WWW1). It can also been downloaded from the University of Maryland Global Land Cover Facility (WWW2). The GLASS FAPAR products from this study will also be available at these two sites. This work was financially supported through grant no. 2013AA121201 under the "State Program for High-Tech Research and Development (863 program)", the Chinese 973 Program under grant no. 2013CB733403 and the National Natural Science Foundation of China under grant nos. 41171264 and 41331173.

References

Baret, F., Hagolle, O., Geiger, B., Bicheron, P., Miras, B., Huc, M., ... Leroy, M. (2007). LAI, fAPAR and fCover CYCLOPES global products derived from VEGETATION: Part 1: Principles of the algorithm. *Remote Sensing of Environment*, *110*(3), 275–286.

Baret, F., Weiss, M., Lacaze, R., Camacho, F., Makhmara, H., Pacholcyzk, P., & Smets, B. (2013). GEOV1: LAI and FAPAR essential climate variables and FCOVER global time series capitalizing over existing products. Part1: Principles of development and production. *Remote Sensing of Environment*, *137*, 299–309.

Carrer, D., Meurey, C., Ceamanos, X., Roujean, J. -L., Calvet, J. -C., & Liu, S. (2014). Dynamic mapping of snow-free vegetation and bare soil albedos at global 1 km scale from 10-year analysis of MODIS satellite products. *Remote Sensing of Environment*, *140*, 420–432.

Camacho, F., Cernicharo, J., Lacaze, R., Baret, F., & Weiss, M. (2013). GEOV1: LAI, FAPAR essential climate variables and FCOVER global time series capitalizing over existing products. Part 2: Validation and intercomparison with reference products. *Remote Sensing of Environment*, *137*, 310–329.

Campbell, S.G., & Norman, J.M. (1998). *An Introduction to Environmental Biophysics* (2nd ed.). New York, NY: Springer-Verlag.

Chen, J., Menges, C., & Leblanc, S. (2005). Global mapping of foliage clumping index using multi-angular satellite data. *Remote Sensing of Environment*, *97*(4), 447–457.

Cukier, R.I., Fortuin, C.M., Schuler, K.E., Petschek, A.G., & Schaibly, J.H. (1973). Study of the sensitivity of coupled reaction systems to uncertainties in rate coefficients: I Theory. *Journal of Chemical Physics*, *59*, 3873–3878.

Cukier, R.I., Levine, H.B., & Schuler, K.E. (1978). Nonlinear sensitivity analysis of multiparameter model systems. *Journal of Computational Physics*, *26*, 1–42.

D'Odorico, P., Gonsamo, A., Pinty, B., Gobron, N., Coops, N., Mendez, E., & Schaepman, M.E. (2014). Intercomparison of fraction of absorbed photosynthetically active radiation products derived from satellite data over Europe. *Remote Sensing of Environment*, *142*, 141–154.

Fensholt, R., Sandholt, I., & Rasmussen, M.S. (2004). Evaluation of MODIS LAI, fAPAR and the relation between fAPAR and NDVI in a semi-arid environment using in situ measurements. *Remote Sensing of Environment*, *91*(490–507), 2004.

Gobron, N., Pinty, B., Verstraete, M.M., & Govaerts, Y. (1999). The MERIS Global Vegetation Index (MGVI): Description and preliminary application. *International Journal of Remote Sensing*, *20*, 1917–1927.

Gobron, N., Mélin, F., Pinty, B., Verstraete, M.M., Widlowski, J.L., & Bucini, G. (2001). A global vegetation index for SeaWiFS: Design and applications. In M. Beniston, & M.M. Verstraete (Eds.), *Remote sensing and climate modeling: synergies and limitations* (pp. 5–21). Dordrecht, The Netherlands: Kluwer Academic Publishers.

Gobron, N., Aussedat, O., & Pinty, B. (2006). MODerate Resolution Imaging Spectroradiometer, JRC-FAPAR Algorithm Theoretical Basis Document. EUR Report No. 22164 EN: Institute for Environment and Sustainability.

Gobron, N., Pinty, B., Aussedat, O., Chen, J.M., Cohen, W.B., Fensholt, R., ... Widlowski, J. -L. (2006). Evaluation of FAPAR products for different canopy radiation transfer regimes: methodology and results using JRC products derived from SeaWiFS against ground-based estimations. *Journal of Geophysical Research*, *111*.

Gobron, N., Pinty, B., Mélin, F., Taberner, M., Verstraete, M., Robustelli, M., & Widlowski, J.L. (2007). Evaluation of the MERIS/ENVISAT FAPAR product. *Advances in Space Research*, *39*, 105–115.

Gower, S.T., Kucharik, C.J., & Norman, J.M. (1999). Direct and indirect estimation of leaf area index, fAPAR, and net primary production of terrestrial ecosystems. *Remote Sensing of Environment*, *70*, 29–51.

He, L., Chen, J.M., Pisek, J., Schaaf, C.B., & Strahler, A.H. (2012). Global clumping index map derived from the MODIS BRDF product. *Remote Sensing of Environment*, *119*, 118–130.

Huemmrich, K.F., Privette, J.L., Mukelabai, M., Myneni, R.B., & Knyazikhin, Y. (2005). Time-series validation of MODIS land biophysical products in a Kalahari woodland, Africa. *International Journal of Remote Sensing*, *26*(19), 4381–4398.

Knyazikhin, Y., Martonchik, J.V., Myneni, R.B., Diner, D.J., & Running, S.W. (1998). Synergistic algorithm for estimation of vegetation canopy leaf area index and fraction of absorbed photosynthetically active radiation from MODIS and MISR data. *Journal of Geophysical Research*, *103*, 32257–32276.

Liang, S., Zhang, X., Xiao, Z., Cheng, J., Liu, Q., & Zhao, X. (2013). *Global LAnd Surface Satellite (GLASS) products: Algorithms, validation and analysis.* Springer.

Liang, S., Zhao, X., Yuan, W., Liu, S., Cheng, X., Xiao, Z., ... Townshend, J. (2013). A long-term Global LAnd Surface Satellite (GLASS) dataset for environmental studies. *International Journal of Digital Earth*, *6*(supp. 1), 5–33.

McCallum, I., Wagner, W., Schmullius, C., Shvidenko, A., Obersteiner, M., Fritz, S., et al. (2010). Comparison of four global FAPAR data sets over northern Eurasia for the year 2000. *Remote Sensing of Environment*, *114*(5), 941–949.

Morisette, J.T., Baret, F., Privette, J.L., Myneni, R.B., Nickeson, J., Garrigues, S., ... Cook, R. (2006). Validation of global moderate-resolution LAI products: A framework proposed within the CEOS Land Product Validation Subgroup. *IEEE Transactions on Geoscience and Remote Sensing*, *44*, 1804–1817.

Myneni, R.B., Hoffman, S., Knyazikhin, Y., Privette, J.L., Glassy, J., Tian, Y., ... Running, S.W. (2002). Global products of vegetation leaf area and fraction absorbed PAR from year one of MODIS data. *Remote Sensing of Environment*, *83*, 214–231.

Pinty, B., Clerici, M., Andredakis, I., Kaminski, T., Taberner, M., Verstraete, M.M., ... Widlowski, J. -L. (2011). Exploiting the MODIS albedos with the Two-stream Inversion Package (JRC-TIP): 2. Fractions of transmitted and absorbed fluxes in the vegetation and soil layers. *Journal of Geophysical Research*, *116*, D09106.

Plummer, S., Arino, O., Simon, W., & Steffen, W. (2006). Establishing an Earth observation product service for the terrestrial carbon community: the GLOBCARBON initiative. *Mitigation and Adaptation Strategies for Global Change*, *11*, 97–111.

Pedelty, J., Vermote, E.F., Devadiga, S., Roy, D., Schaaf, C., Privette, J., et al. (2007). Generating a long-term land data record from the AVHRR and MODIS instruments. *IEEE International Geoscience and Remote Sensing Symposium* (pp. 1021–1025).

Riado, E., Conde, J. R. & Minguez, M., I. (1998). Estimating fAPAR from nine vegetation indices for irrigated and nonirrigated faba bean and semileafless pea canopies. Remote Sensing of Environment, 66, 87–100.

Rechid, D., Raddatz, T.J., & Jacob, D. (2009). Parameterization of snow-free land surface albedo as a function of vegetation phenology based on MODIS data and applied in climate modeling. *Theoretical and Applied Climatology*, *95*(3–4), 245–255.

Ratto, M., Pagano, A., & Young, P. (2007). State dependent parameter metamodelling and sensitivity analysis. *Computer Physics Communications*, *177*(11), 863–876.

Saltelli, A. (2004). *Sensitivity analysis in practice: A guide to assessing scientific models.* Hoboken, NJ: Wiley.

Saltelli, A., Tarantola, S., & Chan, K.P. -S. (1999). A quantitative modelindependent method for global sensitivity analysis of model output. American Statistical Association and the American Society for Quality. *Technometrics*, *41*(1), 39–56.

Serbin, S.P., Ahl, D.E., & Gower, S.T. (2013). Spatial and temporal validation of the MODIS LAI and FPAR products across a boreal forest wildfire chronosequence. *Remote Sensing of Environment*, *133*, 71–84.

Tao, X., Liang, S., & Wang, D. (2015). Assessment of five global satellite products of fraction of absorbed photosynthetically active radiation: Intercomparison and direct validation against ground-based data. *Remote Sensing of Environment*, *163*, 270–285.

Widlowski, J-L., Lavergne, T., Pinty, B., Gobron, N., & Verstraete, M.M. (2008). Towards a high spatial resolution limit for pixel-based interpretations of optical remote sensing data. Advances in Space Research, 41(11), 1724–1732.

Xiao, Z., Liang, S., Wang, J., Chen, P., Yin, X., Zhang, L., & Song, J. (2014). Use of general regression neural networks for generating the GLASS leaf area index product from time series MODIS surface reflectance. *IEEE Transactions on Geoscience and Remote Sensing*, *52*(1), 209–223.

Xiao, Z., Liang, S., Wang, J., Xie, D., Song, J., & Fensholt, R. (2015). A framework for consistent estimation of leaf area index, fraction of absorbed photosynthetically active radiation, and surface albedo from MODIS time-series data. *IEEE Transactions on Geoscience and Remote Sensing*, *53*(6), 3178–3197.

Xiao, Z., Liang, S., Wang, J., Xiang, Y., Zhao, X., & Song, J. (2015). *Long time-series global land surface satellite (GLASS) leaf area index product derived from MODIS and AVHRR data.* IEEE Transactions on Geoscience and Remote Sensing in review.

Yang, W., Tan, B., Huang, D., Rautiainen, M., Shabanov, N.V., Wang, Y., ... Myneni, R.B. (2006). MODIS leaf area index products: From validation to algorithm improvement. *IEEE Transactions on Geoscience and Remote Sensing*, *44*(7), 1885–1898.

WWW sites

(d). The GLASS LAI at Beijing Normal University. http://www.bnu-datacenter.com/en
(d). The GLASS LAI at the Global Land Cover Facility. http://glcf.umd.edu
(d). The MODIS products. http://reverb.echo.nasa.gov/reverb/
(d). The GEOV1 FAPAR product. http://www.geoland2.eu/
(d). The JRC FAPAR product. http://fapar.jrc.ec.europa.eu/Home.php
(d). The VALERI validation data. http://w3.avignon.inra.fr/valeri/
(d). The MODIS user tools. https://www.umb.edu/spectralmass/terra_aqua_modis/modis_user_tools